

Probing the Architecture of an L-type Calcium Channel with a Charged Phenylalkylamine

EVIDENCE FOR A WIDELY OPEN PORE AND DRUG TRAPPING*^[5]

Received for publication, September 26, 2006, and in revised form, November 27, 2006. Published, JBC Papers in Press, November 30, 2006, DOI 10.1074/jbc.M609153200

Stanislav Beyl[‡], Eugen N. Timin[‡], Annette Hohaus[‡], Anna Stary[§], Michaela Kudrnac[‡], Robert H. Guy[¶], and Steffen Hering^{†1}

From the [‡]Institute for Pharmacology and Toxicology, University of Vienna, Althanstrasse 14, A-1090 Vienna, Austria,

[§]Institute of Theoretical Chemistry, University of Vienna, Waehringerstrasse 17, A-1090 Vienna, Austria,

and [¶]Laboratory of Cell Biology, NCI, National Institutes of Health, Bethesda, Maryland 20892-5567

Voltage-gated calcium channels are in a closed conformation at rest and open temporarily when the membrane is depolarized. To gain insight into the molecular architecture of Ca_v1.2, we probed the closed and open conformations with the charged phenylalkylamine (–)devapamil ((–)qD888). To elucidate the access pathway of (–)D888 to its binding pocket from the intracellular side, we used mutations replacing a highly conserved Ile-781 by threonine/proline in the pore-lining segment IIS6 of Ca_v1.2 (1). The shifted channel gating of these mutants (by 30–40 mV in the hyperpolarizing direction) enabled us to evoke currents with identical kinetics at different potentials and thus investigate the effect of the membrane potentials on the drug access *per se*. We show here that under these conditions the development of channel block by (–)qD888 is not affected by the transmembrane voltage. Recovery from block at rest was, however, accelerated at more hyperpolarized voltages. These findings support the conclusion that Ca_v1.2 must be opening widely to enable free access of the charged (–)D888 molecule to its binding site, whereas drug dissociation from the closed channel conformation is restricted by bulky channel gates. The functional data indicating a location of a trapped (–)D888 molecule close to the central pore region are supported by a homology model illustrating that the closed Ca_v1.2 is able to accommodate a large cation such as (–)D888.

The pore-forming α_1 -subunit of voltage-gated Ca²⁺ channels (Ca_v)² is composed of four homologous domains (I–IV), each of which has six transmembrane segments (S1–S6) (2). Membrane depolarization initiates conformational changes leading to channel opening (activation) and subsequent closure

(inactivation). Channel activation can be considered as a multi-step process in which a conformational change in the voltage sensor (formed by multiple charged amino acids located in segment S4 and adjacent structures of each domain (3)) stimulates opening of a gate (formed by the four S6 segments).

Three-dimensional structures of Ca_v are not known. Comparisons of the crystal structures of the closed KcsA (4) and the open conformation of K_v1.2 (5) suggest that pore-forming S6 segments undergo substantial conformational changes during channel activation. Extension of this hypothesis to Ca²⁺ channels is supported by recent kinetic studies on mutant Ca_v1.2 that suggest bending in segment IIS6 during channel activation (1).

Ca_v1.2 channels are highly sensitive to phenylalkylamines (PAA) (6). Here we investigate whether the permanently charged (quaternary) (–)devapamil ((–)qD888) can freely access its binding pocket in the open inner pore of Ca_v1.2 from the intracellular side. To analyze the effect of the membrane potential on channel block, we used mutations of the conserved Ile-781 to threonine/proline in the pore-lining segment IIS6 of Ca_v1.2 (1, 7) that have previously been shown to shift channel activation and inactivation by 30/40 mV in the hyperpolarizing direction (1). The unique kinetic phenotypes of these mutants (displaying similar Ca²⁺ channel current kinetics at different membrane potentials) enabled us to analyze, for the first time, the role of the membrane potential *per se* in Ca_v inhibition by a PAA. The novel findings of this study are that the development of channel block by (–)qD888 is unaffected by the transmembrane voltage, but recovery from block at rest is affected, *i.e.* dissociation accelerates as the voltage becomes more negative. These findings lead us to conclude that drug association occurs via a widely open channel mouth (free access of the charged molecule with no voltage drop from inside to the binding site), whereas drug dissociation from the closed channel conformation is restricted by the closed channel gate that has a substantial voltage drop across it. Analyzing the voltage-dependence of recovery using the Eyring rate constant theory predicts that the quaternary and tertiary (–)D888 bind near the central pore region.

EXPERIMENTAL PROCEDURES

Cell Culture and Transient Transfection—Human embryonic kidney tsA-201 cells were grown at 5% CO₂ and 37 °C to 80% confluence in Dulbecco's modified Eagle's medium/F-12 supplemented with 10% (v/v) fetal calf serum and 100 units/ml

* This work was supported by Fonds zur Förderung der wissenschaftlichen Forschung (Austrian Science Fund) Grant 15914 and by the Intramural Research Program of the NCI, Center for Cancer Research, National Institutes of Health (to R. H. G.). The costs of publication of this article were defrayed in part by the payment of page charges. This article must therefore be hereby marked "advertisement" in accordance with 18 U.S.C. Section 1734 solely to indicate this fact.

^[5] The on-line version of this article (available at <http://www.jbc.org>) contains supplemental Figs. 6 and 7, Table 2, and other supplemental data.

¹ To whom correspondence should be addressed: Inst. for Pharmacology and Toxicology, University of Vienna, Althanstrasse 14, A-1090 Vienna, Austria. Tel.: 43-14277-55310; Fax: 43-14277-9553; E-mail: steffen.hering@univie.ac.at.

² The abbreviations used are: Ca_v, voltage-gated Ca²⁺ channels; PAA, phenylalkylamines; (–)qD888, quaternary (–)devapamil; I_{Bar}, barium currents.

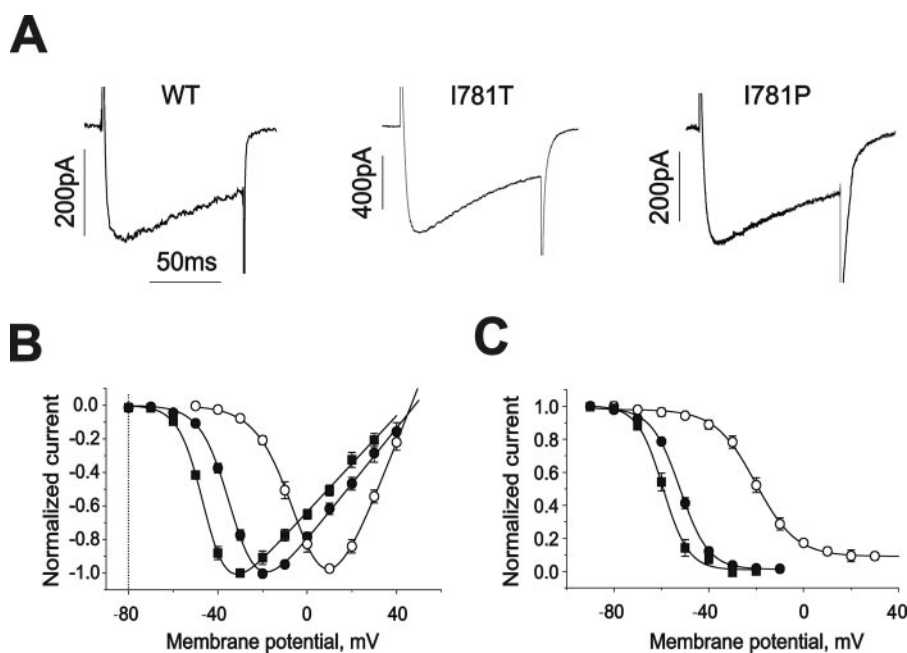


FIGURE 1. Similar kinetics of I_{Ba} through wild-type $Ca_v1.2$ and mutants I781T and I781P at different test potentials. *A*, I_{Ba} currents are evoked by 100 ms test pulses to 20 mV (wild-type), -10 mV (I781T), and -20 mV (I781P) from -80 mV. *B*, normalized current-voltage relationships of the wild-type ($n = 9$, open circles), I781T ($n = 6$, filled circles), and I781P ($n = 6$, filled squares) mutant channels. Potentials of half-maximal activation ($V_{0.5,act}$) are -1.1 ± 0.8 mV, -29.9 ± 0.6 mV, and -44.1 ± 0.7 mV for wild-type, I781T, and I781P mutant channels, respectively. *C*, average voltage dependencies of steady-state inactivation for wild-type ($n = 3$, open circles), I781T ($n = 3$, filled circles), and I781P ($n = 3$, filled squares) mutant channels. Solid lines represent fits to Boltzmann functions. Potentials of half-maximal inactivation ($V_{0.5,inact}$) are -20.0 ± 0.8 mV, -52.1 ± 0.6 mV, and -59.3 ± 1.0 for wild-type, I781T, and I781P mutant channels respectively.

penicillin/streptomycin. Cells were split using trypsin/EDTA and plated on 35-mm Petri dishes (Falcon) at 30–50% confluence ~ 16 h before transfection. Subsequently tsA-201 cells were co-transfected with cDNAs encoding wild-type (GenBankTM accession number X15539) or mutant $Ca_v1.2$ α_1 -subunits (I781P and I781T), (1) with auxiliary β_{1a} (8) as well as α_2 - and δ_1 -subunits (9). The transfection of tsA-201 cells was performed using the FuGENE 6 transfection reagent (Roche Applied Science) following standard protocols.

Ionic Current Recordings and Data Acquisition—Barium currents (I_{Ba}) through voltage-gated Ca^{2+} channels were recorded at 22–25 °C using the patch clamp technique (10) by Axopatch 200A patch clamp amplifier (Axon Instruments) 36–48 h after transfection. The extracellular bath solution contained $BaCl_2$ 20 mM, 1 mM, HEPES 10 mM, and choline-Cl 140 mM, titrated to pH 7.4 with methanesulfonic acid. Patch pipettes with resistances of 1–4 megohms were made from borosilicate glass (Clark Electromedical Instruments) and filled with pipette solution containing CsCl 145 mM, $MgCl_2$ 3 mM, HEPES 10 mM, and EGTA 10 mM, titrated to pH 7.25 with CsOH.

Quaternary (–)devapamil ((–)D888) was synthesized by David Kimball, Bristol-Meyers Squibb (see Ref. 11 for details), and tertiary (–)D888 was from Knoll AG Ludwigshafen. For intracellular application, (–)qD888 was dissolved in the internal (pipette) solution and applied directly via the patch pipette. I_{Ba} were recorded 5 min after the whole cell configuration was established. To assure that that the internal drug concentration reached steady state, use-dependent block was monitored after

different time intervals. An approximation of the time for intracellular perfusion (see Ref. 12) predicts that under our experimental conditions, an equilibrium between the pipette concentration of (–)D888 and the intracellular solution should be reached within about 10 s. Quaternary (–)D888 was applied by conventional bath perfusion from the outside and I_{Ba} recorded after a 5 min equilibration period.

The current-voltage (I - V) curves were fitted using the following modified Boltzmann equation, $I = G_{max} (V - V_{rev}) / (1 + \exp((V_{0.5,act} - V) / k_{act}))$, where V_{rev} is extrapolated reversal potential, V is membrane potential, I is peak current, G_{max} is maximum membrane conductance, $V_{0.5,act}$ is the voltage corresponding to half-maximal activation, and k_{act} is a slope factor.

The voltage-dependence of I_{Ba} inactivation (inactivation curve) was measured using a multi-step protocol to account for run-down (7). The pulse sequence was applied beginning at 40-s intervals from a

holding potential of -80 mV. Steady-state inactivation curves were drawn according to a Boltzmann equation, $I_{Ba,inact} = I_{ss} + (1 - I_{ss}) / (1 + \exp((V - V_{0.5,inact}) / k))$, where V is membrane potential, $V_{0.5,inact}$ is midpoint voltage, k is the slope factor, and I_{ss} is the fraction of non-inactivating current.

Use-dependent Ca^{2+} channel block was estimated as peak I_{Ba} inhibition during short (100 ms) test pulses from -80 mV at a frequency of 0.2 Hz. The dose-response curves of I_{Ba} inhibition were fitted using the Hill equation, $I_{Ba,drug} / I_{Ba,control}$ (in %) = $(100 - A) / (1 + (C / IC_{50})^{n_H}) + A$, where IC_{50} is the concentration at which I_{Ba} inhibition is half-maximal, C is the applied drug concentration, A is the fraction of I_{Ba} that is not blocked, and n_H is the Hill coefficient.

I_{Ba} -unblock from use-dependent inhibition by (–)qD888 or (–)D888 was studied by applying a 20-ms test pulse at various time intervals after the last pulse of the train. The time course of I_{Ba} recovery from block was fitted to a mono-exponential function. Recovery from slow inactivation was measured by applying a 6-s prepulse and subsequently 20-ms test pulses at increasing time intervals starting at 0.3 s after the prepulse to skip recovery from fast inactivation.

All data were digitized using a DIGIDATA 1200 interface (Axon Instruments), smoothed by means of a four-pole Bessel filter, and stored on computer hard disc. 100-ms current traces were sampled at 10 kHz and filtered at 5 kHz; for the steady-state inactivation protocol, currents were sampled at 1 kHz and filtered at 0.5 kHz. Leak currents were subtracted digitally using average values of scaled leakage currents elicited by a 10-mV hyperpolarizing pulse. Series resistance and offset voltage were

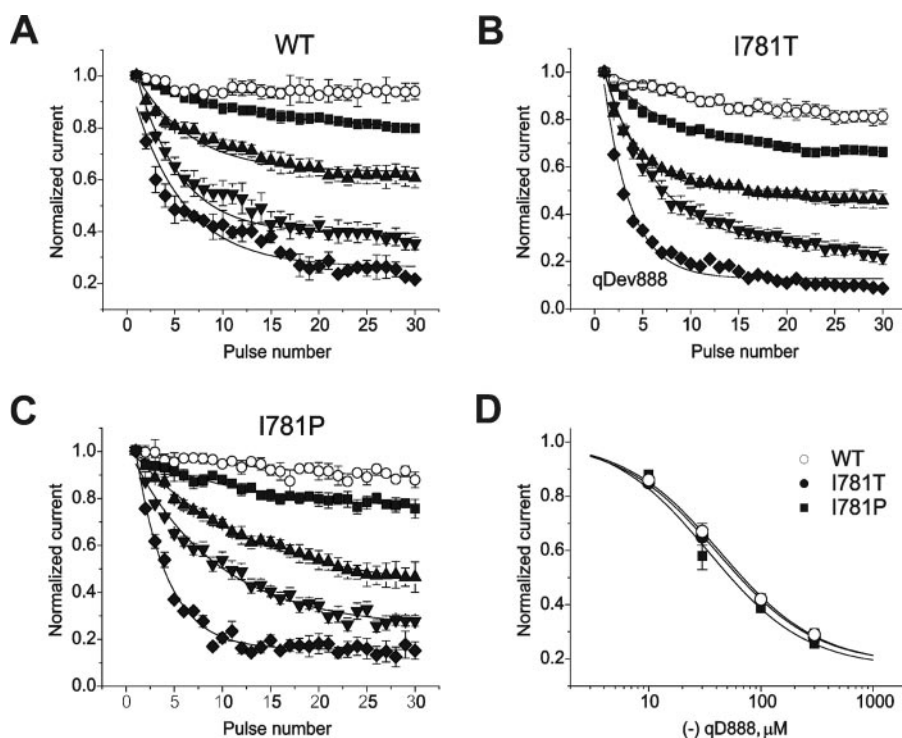


FIGURE 2. Similar inhibition of wild-type, I781T, and I781P mutant channels by (-)qD888. *A*, *B*, and *C*, use-dependent block of wild-type (*A*), I781T (*B*), and I781P (*C*) mutant channels by different concentrations of the calcium channel blocker (-)qD888. Use-dependent inhibition of wild-type and mutant channels was measured in the absence (○) or presence of 10 μM (■), 30 μM (▲), 100 μM (▼), or 300 μM (◆) (-)qD888 in the pipette (intracellular) solution. Channel block was estimated as peak I_{Ba} inhibition during trains of 30 pulses (0.2 Hz, 100 ms) applied from a holding potential of -80 mV to +20 mV (wild-type), -10 mV (I781T) or -20 mV (I781P). *D*, concentration dependence of peak I_{Ba} inhibition by (-)qD888 in wild-type (○), I781T (●), and I781P (■) mutant channels. Channel block was estimated as the difference between “steady state” normalized current in control and in presence of (-)qD888. Data points are the mean from 3–6 experiments. The IC_{50} values were obtained by fitting the data points to the Hill equation (as described under “Experimental Procedures”) yielding $43.7 \pm 3.4 \mu\text{M}$ (wild-type), $41.0 \pm 2.1 \mu\text{M}$ (I781T), and $34.3 \pm 8.2 \mu\text{M}$ (I781P).

routinely compensated for. The pClamp software package (version 7.0 Axon Instruments, Inc.) was used for data acquisition and preliminary analysis. Microcal Origin 7.0 was used for analysis and curve fitting. Data are given as mean \pm S.E. for $n \geq 4$. Statistical significance was assessed with Student’s unpaired *t* test.

RESULTS

We have previously shown that amino acid substitutions for Ile-781 in segment IIS6 ($Ca_v1.2$) shift the channel activation and inactivation curves by similar amounts in the hyperpolarizing direction (1). Mutants I781T and I781P display the most prominent changes in gating. Here we use these mutants to analyze whether the access of a large cation, such as the permanently charged PAA (-)qD888, to its putative binding site near the central cavity of the $Ca_v1.2$ (13–16) is affected by the transmembrane voltage. This question could not be answered using wild-type channels because changes in current kinetics (at different test potentials) substantially alter the rate and amount of channel inhibition (see Refs. 17–19 for review). The fact that mutants I781T and I781P activate and inactivate with similar kinetics at different membrane potentials enabled us to eliminate effects of state-dependent drug action while analyzing channel block at different voltages.

We used a 4-fold higher Ba^{2+} concentration (20 mM) than in Hohauser *et al.* (1) to better resolve I_{Ba} in the presence of high

concentrations of intracellular (-)qD888. I_{Ba} traces the corresponding current-voltage, and the inactivation curves are shown in Fig. 1, *A–C*. Shifts in the midpoint voltage of activation and inactivation curves and similar reversal potentials of the channels agree with our previous study (1). A comparison of the current kinetics (Fig. 1*A*) during 100 ms pulses to different test potentials (20 mV in wild-type, -10 mV in I781T and -20 mV in I781P), where channel activation reaches a maximal value, confirmed that the channels activated ($\tau_{m,wt} = 4.0 \pm 0.6$ versus $\tau_{m,I781T} = 3.7 \pm 0.7$ and $\tau_{m,I781P} = 4.2 \pm 0.6$) and inactivated ($43 \pm 8\%$ (wild type) versus $46 \pm 5\%$ (I781T) and $40 \pm 7\%$ (I781P)) at these potentials with almost identical kinetics.

(-)qD888 Binds in a Use-dependent and Voltage-independent Manner—It is widely accepted that charged PAA access their binding site in the open channel pore from the intracellular side via a hydrophilic route (e.g. 11, 20). Consistent with this assumption, (-)qD888 inhibited wild-type $Ca_v1.2$ and mutants I781T and I781P in a use-dependent manner. The develop-

ment of channel inhibition at the three test potentials 20 mV (wild type), -10 mV (I781T), and -20 mV (I781P) during 0.2-Hz pulse trains is shown in Fig. 2. We observed a current inhibition of wild-type channels by $20 \pm 2\%$ (10 μM), $39 \pm 5\%$ (30 μM), $64 \pm 4\%$ (100 μM), and $77 \pm 4\%$ (300 μM) compared with $34 \pm 2\%$, $54 \pm 5\%$, $77 \pm 4\%$, and $91 \pm 4\%$ in I781T and $23 \pm 2\%$, $53 \pm 7\%$, $72 \pm 4\%$, and $85 \pm 4\%$ in I781P channels ($n \geq 3$; Fig. 2, *A–C*). Similar current inhibition by 100 μM (-)qD888 was observed at lower (5 mM) barium concentration for wild-type ($66 \pm 3\%$) and I781T ($78 \pm 3\%$).

In drug-free solution, channels accumulated in an inactivated state causing I_{Ba} inhibitions of $6 \pm 5\%$ in wild type, $19 \pm 4\%$ in I781T, and $11 \pm 5\%$ in I781P. After correction for inactivation, drug sensitivities at different voltages were analyzed by plotting steady-state I_{Ba} inhibition versus the applied drug concentration. The time constants of channel block of current inhibition at the different drug concentrations are given in Table 1.

The IC_{50} values for I_{Ba} inhibition of wild-type, I781T and I781P were $43.7 \pm 3.4 \mu\text{M}$, $41.0 \pm 2.1 \mu\text{M}$, and $34.3 \pm 8.2 \mu\text{M}$, respectively (Fig. 2*D*). These data show that the 30 or 40 mV larger test pulses did not enhance I_{Ba} inhibition by (-)qD888, demonstrating that drug access to the binding site was not affected by membrane potential.

Voltage-dependent Recovery from Block Reflects Restricted Drug Dissociation—Fig. 3 illustrates recovery from use-dependent inhibition by (–)qD888 (100 μM) at different holding potentials. Use-dependent block was induced by a standard train (as shown in Fig. 2), and the holding potential thereafter was switched either to -80 , -90 , -100 , or -110 mV. The fraction of recovered channels was determined by applying a test pulse (to 20 mV in wild-type, -10 mV in I781T, and -20 mV in I781P) after different time intervals (see inset in Fig. 3).

I_{Ba} recovered faster at more hyperpolarized potentials (Fig. 3). Plotting the time constants of recovery versus voltage in semi-logarithmic coordinates revealed an exponential dependence (Fig. 3D). Surprisingly, all three channel types recovered at similar voltages with similar time courses despite the different pore stability of the channel constructs (1). Analogous observa-

tions were made when 10 μM tertiary (–)D888 was applied from the extracellular side to cells expressing either wild-type $\text{Ca}_v1.2$ or the mutant I781T (Fig. 4, A and B). At this concentration, about 80% of current inhibition was induced by a standard pulse train. Recovery was voltage-dependent and displayed a similar exponential dependence of the time constant for recovery on the membrane potential (compare Figs. 3D and 4C).

These data suggest that gate structures of the closed conformation form a substantial barrier that is rate-limiting for channel unblock. In other words, increasing the voltage drop across the closed channel gates facilitates the release of (–)D888. If so, the fraction of the membrane voltage affecting dissociation of the trapped drug molecule can be calculated by Eyring theory. This analysis predicts a location of the charged PAA molecule close to the central pore region (see supplemental data and Fig. 5).

Slow Recovery from Block Does Not Reflect Recovery from Slow Inactivation—The experiments in Figs. 3 and 4 were designed to study channel block under conditions minimizing the development of slow inactivation. In analogy to sodium channel block by local anesthetics (21), one could hypothesize that drug binding promotes slow inactivation. This would explain elegantly the voltage-dependent slow recovery observed in Figs. 3 and 4. To analyze a possible role of slow inactivation we compared the voltage-dependencies of recovery from slow inactivation (induced by 6-s depolarizations) and recovery from use-dependent block in wild-type, I781T, and I781P channels (Fig. 6 in supplemental data). Recovery from slow inactivation occurred at a 3–4-fold faster rate at similar holding potentials and showed no strong voltage-dependence (compare Figs. 3 and 4 with Fig. 6 and Table 2 in supplemental data).

DISCUSSION

Our results lead us to conclude that association of D888 is voltage-independent, whereas drug dissociation from closed channels is voltage-dependent.

Evidence for Voltage-independent Access of D888 via a Widely Open Pore Conformation—All three $\text{Ca}_v1.2$ variants (wild-type, I781T, I781P) were blocked to comparable extents (Fig. 2) despite the differences of up to 40 mV in membrane depolarizations applied to induce similar (maximal) activation during the pulse trains (Fig. 1B, arrows). The two mutations (I781T, I781P) did not affect the PAA binding pocket (13–17, 22, 23), as can be seen from similar concentration-dependence of channel inhibition (Fig. 2D). The main effect of these mutations is the pronounced shift in the voltage-dependence of $\text{Ca}_v1.2$ gating (Fig. 1).

TABLE 1

Time constants of peak I_{Ba} inhibition

The time constants of channel block and the different steady-state values of current inhibition at the different drug concentrations shown in Fig. 2.

Concentration of (–)qD888 μM	τ peak I_{Ba} inhibition		
	Wild type	I781T	I781P
10	52.7 ± 4.4	41.6 ± 2.1	52.9 ± 6.5
30	28.2 ± 2.1	19.6 ± 0.5	31.5 ± 3.9
100	22.6 ± 1.2	27.9 ± 1.4	28.9 ± 0.8
300	26.5 ± 3.3	14.0 ± 0.9	16.2 ± 0.7

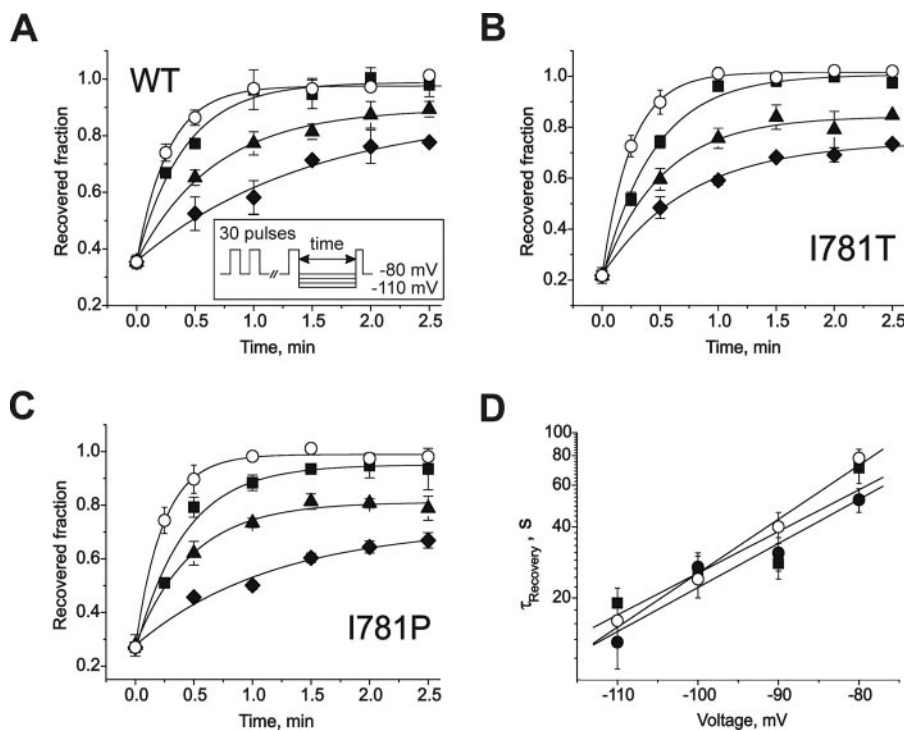


FIGURE 3. Voltage-dependent recovery from block by 100 μM intracellular (–)qD888. A, B, and C, I_{Ba} recovery from block by 100 μM intracellular (–)qD888 of wild-type (A), I781T (B), and I781P (C) mutant channels at holding potentials of -110 (\circ), -100 (\blacksquare), -90 (\blacktriangle), or -80 mV (\blacklozenge). Inset, block was elicited by a standard conditioning train of 30 pulses (see also Fig. 2) and recovery measured applying test pulses at different time after the conditioning train. Data points were fitted by mono-exponential functions; yielding time constants: $\tau_{-110} = 16 \pm 3$ s, $\tau_{-100} = 24 \pm 4$ s, $\tau_{-90} = 40 \pm 6$ s, and $\tau_{-80} = 78 \pm 7$ s for wild-type; $\tau_{-110} = 13 \pm 3$ s, $\tau_{-100} = 27 \pm 4$ s, $\tau_{-90} = 31 \pm 5$ s, and $\tau_{-80} = 52 \pm 6$ s for I781T mutant; $\tau_{-110} = 19 \pm 3$ s, $\tau_{-100} = 25 \pm 5$ s, $\tau_{-90} = 28 \pm 4$ s, and $\tau_{-80} = 71 \pm 10$ s for I781P mutant. D, semi-logarithmic plot of the recovery time constants versus holding potentials. Regression lines yield slopes of 0.022 mV^{-1} (wild-type), 0.018 mV^{-1} (I781T), and 0.017 mV^{-1} (I781P).

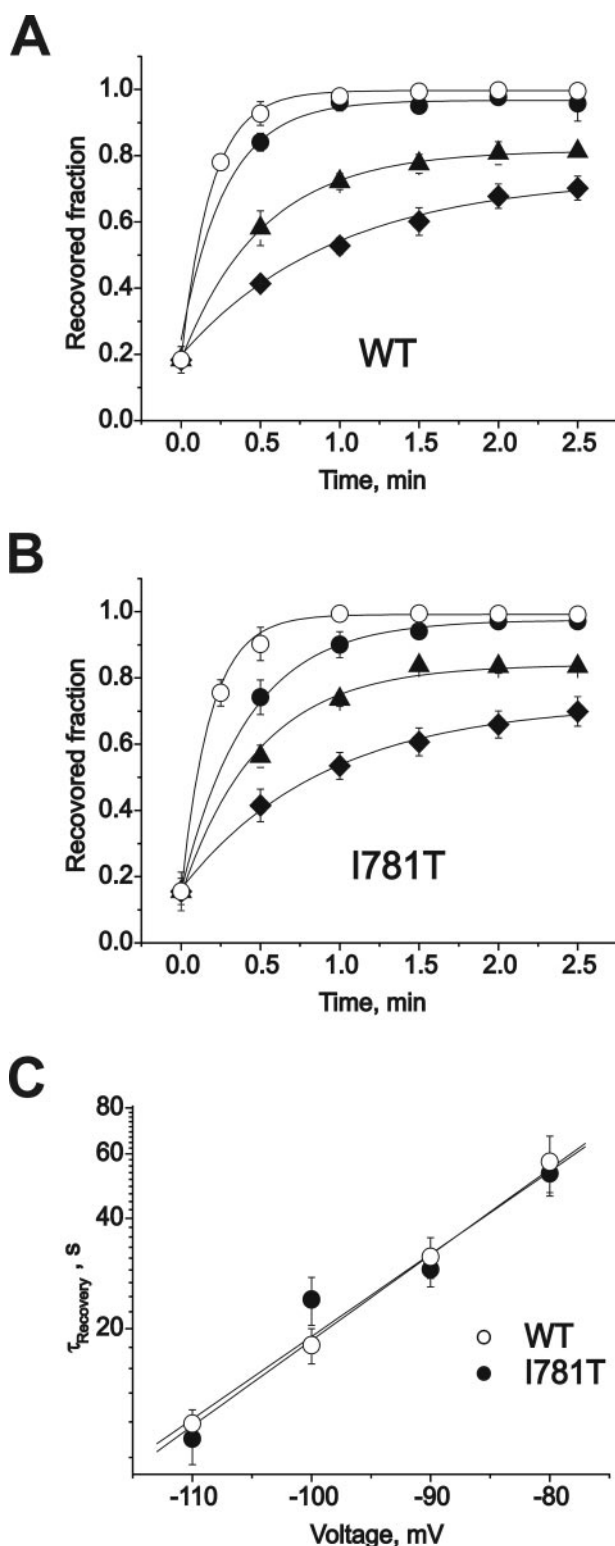


FIGURE 4. Voltage-dependent recovery from block by 10 μM (-)D888. A and B, I_{Ba} recovery from block (10 μM (-)D888) of wild-type (A) and I781T (B) channels at holding potentials of -110 (○), -100 (■), -90 (▲), or -80 mV (◆) (same protocol as described in the legend to Fig. 3). Data points were fitted by mono-exponential functions yielding time constants: $\tau_{-110} = 11 \pm 1$ s, $\tau_{-100} = 18 \pm 2$ s, $\tau_{-90} = 31 \pm 4$ s, and $\tau_{-80} = 57 \pm 10$ s for wild-type; $\tau_{-110} = 10 \pm 1$ s, $\tau_{-100} = 24 \pm 4$ s, $\tau_{-90} = 29 \pm 3$ s, and $\tau_{-80} = 53 \pm 7$ s for I781T mutant. C, semi-logarithmic plot of the recovery time constants versus holding potentials. Regression yields slopes of 0.023 mV^{-1} (wild-type) and 0.022 mV^{-1} (I781T).

The question of voltage-dependence of drug binding cannot be analyzed in wild-type channels because stepping to different test potentials evokes currents with different kinetics, which would inevitably affect use-dependent channel inhibition. Here we made use of mutant $\text{Ca}_v1.2$ channels that activated (and inactivated) at different membrane potentials but with similar kinetics (Fig. 1). These mutants allowed us to analyze blockade of channels for which the fractions of open and inactivated channels were similar but the voltages were different.

Quaternary (permanently charged) PAA such as (-)qD888 enter and block open $\text{Ca}_v1.2$ pores from the intracellular side (11, 20). At a first glance, voltage-independent drug access could be explained by a drug binding site located close to the inner channel mouth. Several results suggest, however, that the putative binding determinants are more likely to be located deeper in the channel pore (13–17, 22, 23).

We believe the voltage-independent access of (-)D888 (Fig. 2) is best explained by a model in which the open inner pore is so wide that the voltage drop between the drug binding site and the intracellular surface of the membrane is negligible. Using the dimensions of the inner channel mouth of an open voltage-gated potassium channel, we calculate a voltage drop of less than 1 mV (Fig. 7 in supplemental data), which would have little effect on the charged drug molecule. This explanation is also supported by a Poisson calculation revealing that the electric field in an open potassium channel is compressed to the selectivity filter (5).

Evidence for Trapping of (-)D888 in the Closed Channel—The drug enters the channel in a voltage-independent manner, and the channel can close while the drug is still bound. There are two ways the drug could leave the closed channel. In scenario 1 the drug can exit the channel only when the channel flickers to a more open conformation, and the voltage-dependence of dissociation is because of voltage-dependence of the conformational change. In scenario 2, channel closure does not completely trap the drug, but it does present a barrier that the drug must pass when it exits the pore. There is a voltage drop across this barrier (because the pore is smaller than in the open conformation), and the voltage-dependence of recovery from blockade is because of the movement of the charged drug through this electric field.

Scenario 1 is unlikely because stronger hyperpolarization decreases the probability of channel flickering to a more open conformation. Figs. 3 and 4 illustrate, however, the facilitation of channel unblock at more hyperpolarized voltages. Our data support therefore scenario 2 in which the slow voltage-dependent dissociation is because of a substantial voltage drop across the closed S6 gate, *i.e.* negative voltages apparently facilitate movement of the charged drug molecule from a central binding site through the closed gate. The exponential dependence of the recovery time constants on membrane potential suggests that an absolute rate constant theory is applicable (see supplemental data). The calculated fractions of the membrane potential affecting drug dissociation range from 0.44 (I781P) to 0.56 (wild-type). Assuming a quasi-linear distribution of the potential within the closed channel, this suggests that the charged molecule binds near the central pore region. A similar fraction

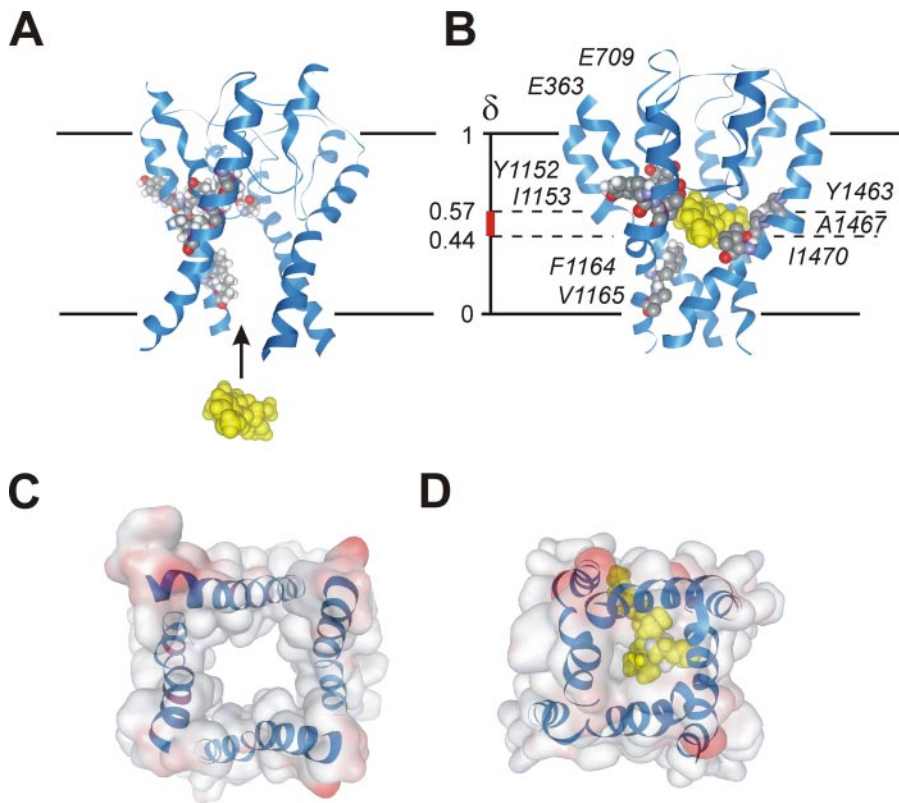


FIGURE 5. Illustration of the drug binding hypothesis in a homology model of $\text{Ca}_v1.2$ in the open (A) and closed (B) channel conformations. Nine determinants of PAA sensitivity in segments III_{S6}, IV_{S6}, and the selectivity filter are indicated (amino acid numbering according to Dilmac *et al.* (16)). A, the model illustrates free access of the permanently charged (–)qD888 molecule (yellow) via a widely open inner channel mouth. B, the figure illustrates one possible conformation of (–)qD888 in the closed $\text{Ca}_v1.2$. The model supports the hypothesis that this compound fits into the cavity of the closed channel pore. The position of the charged molecule within the closed channel conformation (δ ranging from 0.44 to 0.57) was deduced from the voltage dependence of I_{Ba} recovery (Figs. 3, 4, and supplemental data). The precise location and orientation of the drug within the binding pocket remain unknown. Our data support the hypothesis of drug binding to the central pore region (supplemental data). C, bottom surface view of open pore. D, bottom surface view of closed channel pore accommodating (–)qD888.

of 0.56–0.57 was estimated for the tertiary PAA (–)D888 (Fig. 4 and supplemental data).

Closed $\text{Ca}_v1.2$ May Accommodate (–)D888—Our functional data suggest that the channel can close while (–)D888 is bound. We developed homology models of the $\text{Ca}_v1.2$ α_1 subunit to determine whether this hypothesis is consistent with current knowledge of voltage-gated channel structure. Crystal structures of KcsA (4) and $\text{K}_v1.2$ were used as templates to develop models of $\text{Ca}_v1.2$ in closed and open conformations (Ref. 5 and supplemental data). Fig. 5B illustrates that (–)D888 can indeed fit into the cavity of a closed $\text{Ca}_v1.2$. Although modeling of the precise mechanism of drug binding was not attempted, the model clearly illustrates that the spatial requirements for trapping (–)D888 are fulfilled and that the opening through the closed gate is narrow and hydrophobic. The large opening through the model of the inner pore region of the open conformation nicely illustrates the structural basis of voltage-independent drug access.

Summary and Outlook—Our objectives were to gain insights into the architecture of the inner pore region of $\text{Ca}_v1.2$ and to better understand the mechanism by which drugs block these pores from the inside. Our data support the hypothesis that the gates of $\text{Ca}_v1.2$ channels open widely enough to enable

unrestricted (voltage-independent) access of a large molecule such as (–)D888. The above results support a mechanism in which (–)D888 enters the pore and binds in a centrally located cavity in a voltage-independent manner and is subsequently trapped when the channel closes. Although we have not attempted to model the conformation of the blocking molecule nor its precise interaction with the channel, a central cavity in our homology model of a closed $\text{Ca}_v1.2$ can accommodate a large cation such as (–)D888 (Fig. 5). The predicted position of (–)D888 in the cavity would allow interactions with amino acids that have been previously identified as determinants of PAA sensitivity.

The molecular events during channel block are obviously more sophisticated than a simple open channel block. In the present study, we analyzed the mechanism of channel block and unblock by (–)D888 under experimental conditions that minimize the role of inactivation. It is, however, well established that inactivation modulates $\text{Ca}_v1.2$ inhibition by PAA (17, 24–26). Such modulation was recently confirmed in experiments on recombinant channels. Point

mutations within the Ca_v α_1 -subunit that affected the kinetics of inactivation also modulated channel block irrespective of whether the substituted residue was near (within) the putative drug binding pocket or far away (Ref. 19 for review). However, our study clearly illustrates that use-dependent block by (–)D888 is not caused by an accumulation of channels in a slow inactivated state (Fig. 6 in supplemental data). Elucidation of the modulatory effect of inactivation determinants on $\text{Ca}_v1.2$ channel block remains a challenge for future studies.

Acknowledgment—We thank Hannelore Kadlec for excellent technical assistance.

REFERENCES

- Hohaus, A., Beyl, S., Kudrnac, M., Berjukow, S., Timin, E. N., Marksteiner, R., Maw, M. A., and Hering, S. (2005) *J. Biol. Chem.* **280**, 38471–38477
- Catterall, W. A. (2000) *Neuron* **26**, 13–25
- Bezannila, F. (2000) *Physiol. Rev.* **80**, 555–592
- Doyle, D. A., Morais Cabral, J., Pfuetzner, R. A., Kuo, A., Gulbis, J. M., Cohen, S. L., Chait, B. T., and MacKinnon, R. (1998) *Science* **280**, 69–77
- Jiang, Y., Lee, A., Chen, J., Cadene, M., Chait, B. T., and MacKinnon, R. (2002) *Nature* **417**, 523–526
- Catterall, W. A., Perez-Reyes, E., Snutch, T. P., and Striessnig, J. (2005) *Pharmacol. Rev.* **57**, 411–425

Calcium Channel Architecture

- Hemara-Wahanui, A., Berjukow, S., Hope, C. I., Dearden, P. K., Wu, S. B., Wilson-Wheeler, J., Sharp, D. M., Lunden-Treweek, P., Clover, G. M., Hoda, J. C., Striessnig, J., Marksteiner, R., Hering, S., and Maw, M. A. (2005) *Proc. Natl. Acad. Sci. U. S. A.* **102**, 7553–7558
- Ruth, P., Rohrkasten, A., Biel, M., Bosse, E., Regulla, S., Meyer, H. E., Flockerzi, V., and Hofmann, F. (1989) *Science* **245**, 1115–1118
- Ellis, S. B., Williams, M. E., Ways, N. R., Brenner, R., Sharp, A. H., Leung, A. T., Campbell, K. P., McKenna, E., Koch, W. J., Hui, A., Schwartz, A., and Harpold, M. M. (1988) *Science* **241**, 1661–1664
- Hamill, O. P., Marty, A., Neher, E., Sakmann, B., and Sigworth, F. J. (1981) *Pflugers Arch.* **391**, 85–100
- Berjukov, S., Aczel, S., Beyer, B., Kimball, S. D., Dichtl, M., Hering, S., and Striessnig, J. (1996) *Br. J. Pharmacol.* **119**, 1197–1202
- Mathias, R. T., Cohen, I. S., and Oliva, C. (1990) *Biophys. J.* **58**, 759–770
- Hering, S., Aczel, S., Grabner, M., Doring, F., Berjukow, S., Mitterdorfer, J., Sinnegger, M. J., Striessnig, J., Degtiar, V. E., Wang, Z., and Glossmann, H. (1996) *J. Biol. Chem.* **271**, 24471–24475
- Hockerman, G. H., Peterson, B. Z., Johnson, B. D., and Catterall, W. A. (1997) *Annu. Rev. Pharmacol. Toxicol.* **37**, 361–396
- Hockerman, G. H., Johnson, B. D., Abbott, M. R., Scheuer, T., and Catterall, W. A. (1997) *J. Biol. Chem.* **272**, 18759–18765
- Dilmac, N., Hilliard, N., and Hockerman, G. H. (2004) *Mol. Pharmacol.* **66**, 1236–1247
- Hering, S., Aczel, S., Kraus, R. L., Berjukow, S., Striessnig, J., and Timin, E. N. (1997) *Proc. Natl. Acad. Sci. U. S. A.* **94**, 13323–13328
- Hering, S., Berjukow, S., Aczel, S., and Timin, E. N. (1998) *Trends Pharmacol. Sci.* **19**, 439–443
- Hering, S. (2002) *Trends Pharmacol. Sci.* **23**, 509–513
- Hescheler, J., Pelzer, D., Trube, G., and Trautwein, W. (1982) *Pflugers Arch.* **393**, 287–291
- Khodorov, B. I., Peganov, E. M., Revenko, S. V., and Shishkova, L. D. (1975) *Brain Res.* **84**, 541–546
- Hockerman, G. H., Johnson, B. D., Scheuer, T., and Catterall, W. A. (1995) *J. Biol. Chem.* **270**, 22119–22122
- Striessnig, J., Grabner, M., Mitterdorfer, J., Hering, S., Sinnegger, M. J., and Glossmann, H. (1998) *Trends Pharmacol. Sci.* **19**, 108–115
- McDonald, T. F., Pelzer, D., and Trautwein, W. (1984) *J. Physiol. (Lond.)* **352**, 217–241
- Uehara, A., and Hume, J. R. (1985) *J. Gen. Physiol.* **85**, 621–647
- Sanguinetti, M. C., and Kass, R. S. (1984) *Circ. Res.* **55**, 336–348